Journal of Genetic Engineering and Biotechnology 16 (2018) 115–124

HOSTED BY

Contents lists available at ScienceDirect

Journal of Genetic Engineering and Biotechnology

journal homepage: www.elsevier.com/locate/jgeb

Original Article

Green synthesis of zero valent colloidal nanosilver targeting A549 lung cancer cell: In vitro cytotoxicity

Minakshi Jha, Navinchandra G. Shimpi *

Department of Chemistry, University of Mumbai, Santacruz (East), Mumbai 400098, India

ARTICLE INFO

Article history:
Received 5 July 2017
Received in revised form 20 December 2017
Accepted 29 December 2017
Available online 5 January 2018

Keywords:
M. charantia
Silver nanoparticles
TEM
Anticancer activity
A549
HOP-62

ABSTRACT

An eco-friendly green approach was proposed to synthesise stable, cytotoxic colloidal silver nanoparticles (AgNPs) using *Momordica charantia* (*M. charantia*) fruit extract. Bioinspired green method adopted for fabrication of AgNPs because of easy, fast, low-cost and benign bioprocess. Phytocomponents played the crucial role in capping, stabilisation and inherent cytotoxic potential of colloidal nanosilver. The physiochemical, crystalline, optical and morphological properties of AgNPs were characterized using UV-vis, FT-IR, XRD, SEM, TEM, EDX and AFM. FT-IR reveals the presence of carbonyl, methyl, polyphenol (flavonoid), primary and secondary amine (protein), carboxyl group, ester as major functional groups over the surface of nanomaterials. Mechanistic pathway for formation and stabilisation of colloidal nanosilver has been discussed. Average crystalline size of AgNPs was found to be 12.55 nm from XRD. TEM shows AgNPs nanosphere with size range 1–13.85 nm. Consistency in spherical morphology was also confirmed through Atomic Force Microscopy (AFM). AFM measurement provided image Rq value 3.62, image Ra 2.47, roughness Rmax 36.4 nm, skewness 1.99 and kurtosis 9.87. The SRB assay revealed substantial *in vitro* noticeable anti-cancer activity of colloidal nanosilver on A549 and HOP-62 human lung cancer cells in a dose dependent manner with IC50 value of 51.93 μg/ml and 76.92 μg/ml. In addition, *M. charantia* capped AgNPs were found to be more biocompatible in comparison to *M. charantia* FE. Our study demonstrated the integration of green chemistry principle in nanomaterials fabrication and focused on the potential use of *M. charantia* fruit extract as an efficient precursor for biocompatible AgNPs anodrug formulation with improved cytotoxic applications.

1. Introduction

Now-a-days development of novel nanomaterial with innate potential in nanomedicine field, fabrication of green synthesised nanocarrier possessing the capability of targeted delivery of drug in controlled manner without damaging normal cells is the dream of researchers. Due to high surface to volume ratio, stability, enhanced interaction, and excellent reactivity, the field of nanotechnology has blossomed with development of targeted nanodrug as a promising candidate for medicinal applications [1,2]. In recent years, nanotechnology is a flourishing area and there has been a great demand for plant mediated natural nanomedicine for chemoprevention in the pharmaceutical and biotechnology field. Fabrication of nanocarrier drug by green synthetic approach is a sustainable initiative, required to minimise side effects and improved therapeutic efficiency to protect next generation. In present scenario, lung cancer is the most recurrent reason of cancer deaths worldwide, followed by breast cancer [3,4]. Now-a-days, radiotherapy (side effect- fatal damage, skin problem, hair loss and secondary malignancy) and chemotherapy (side effect- nephrotoxicity, cardiotoxicity, hypersensitivity) is the most reliable and recommended treatment for cancer, which is based on systematic administration of bolus doses of drugs to cancer patients [5] However, the existing cytotoxic drugs owing to their bulky polycyclic structure [6] and high lattice energy, causes inability to form hydrogen bond with water and lack of water solubility is a key obstacle towards accurate delivery of drug. As per the Biopharmaceutics Classification System, a drug could be inefficiently aqueous soluble if its highest dose strength is not soluble in 250 ml over the pH range of 1–7.51 [7]. Unfortunately, many existing cytotoxic drugs fall in this category. In this perspective, green synthesis of novel zero-valent colloidal nanosilver as anticancer drug, is an effective strategy and promising alternative towards accurate nanodelivery of dose without any side effect.

Peer review under responsibility of National Research Center, Egypt.
* Corresponding author.
E-mail address: navin_shimpi@rediffmail.com (N.G. Shimpi).

https://doi.org/10.1016/j.jgeb.2017.12.001
1687-157X/

Among diverse metal nanoparticles, we fabricated silver nanoparticles (AgNPs) which had established a superior phenomenal impact and proved as the most promising candidate for various application in emerging fields such as catalysis [8], medicine [9], drug delivery, diagnosis and imaging [10] and photonics [11], owing to their unique electrical, optical, thermal, physical and chemical properties [12]. Recently silver nanoparticles have been synthesised using *Butea monosperma* [13], *Taxus yunnanensis Callus* [14], *Lonicera hypoglauca* [15], *Phoma glomerata* [16] *Ficus benghalensis* and *Azadirachta indica* [17] extracts. Green synthesis was favoured over conventional chemical and physical synthetic methods because of naturally occurring reducing agent which is safe, eco-friendly, cost effective, less time consuming during processing, less hazardous, no need of high temperature and pressure and no any toxic chemical is required. Furthermore, green extract frequently offers wholesome manipulation and control over nanocrystal growth and stabilisation [17,18].

This study reports green synthesis of AgNPs using *Momordica charantia (M. charantia)* fruit extract, its complete characterizations and evaluation of its innate *in vitro* cytotoxic ability. *M. charantia* belongs to cucurbitaceae family commonly known as bitter melon, balsam pear, bitter gourd, bitter squash or karela. Natural phytocomponents responsible for medicinal properties are flavonoids, saponins, lectins, protein, steroid, triterpene, phenolic compound and alkaloid [19]. Utilisation of nanomaterial in biomedical field for development of chemotherapeutic agent without any side effect is of considerable importance because AgNPs inhibits cell division through apoptotic pathway resulting in damage of cancerous cell. V. Gandhiraj et al. has reported anticancer effect of *M. charantia* leaf extract mediated AgNPs against MCF-7 cell line [20]. B. Ajita and co-workers synthesised AgNPs using leaves extract of *M. charantia* for antimicrobial application [21]. Up to now, there has been no report on *M. charantia* fruit extract (FE) capped AgNPs cytotoxic efficacy against A549 and HOP-62 human lung adenocarcinoma.

2. Experimental work

2.1. Chemicals and culture media

Analytical grade silver nitrate ($AgNO_3 \geq 99.9\%$) was procured from s. d. fine chemicals limited, Mumbai (India) and used without further purification. DMSO supplied by Hi-media, India. Source of A549 and HOP-62 human lung cancer cell line was NCCS, Pune. RPMI 1640, Adriamycin and trichloroacetic acid (TCA) were procured from sigma Aldrich. L-glutamine and all other chemicals were procured from Merck Ltd. Mumbai (India). 10 mg/ml bovine insulin in 25 mM HEPES, p^H 8.2 was procured from sigma cat. no I0516. In addition, 2.5% (wt/vol) trypsin solution was purchase from Invitrogen, cat No. P0290. Sulforhodamine B (SRB), we procured from fluka, (cat No. 86,183) in 1% (vol/vol) acetic acid. Deionised (DI) water and ethanol was used as solvent during synthesis. Solvents were distilled prior to use. The required glassware, used during experiment was carefully acid washed and given a rinse with deionised water. Fresh *M. charantia* fruits were purchased from local market, kalina, Mumbai for the synthesis of silver nanoparticles (AgNPs).

2.2. Extract preparation and synthesis of M. Charantia AgNPs

M. charantia fruit was washed several times with double distilled water along with freshly prepared hot deionised water to remove contaminants from the surface. The fruits were chopped into small pieces with removed seeds. 40 g of fine chopped fruit was added in 300 ml solution (250 ml DI water and 50 ml ethanol) and refluxed at 30^0 for 60 min. Later fruit extract (F.E.) was filtered through whatman No. 1 filter paper and filtrate was stored at 4 °C for further synthesis. In synthetic procedure 100 ml stock solution of $AgNO_3$ (1mM) in DI water was prepared and kept in dark to avoid photoactivation. The overall reaction procedure was carried out in dark to avoid unnecessary photochemical reaction. In a typical synthetic procedure 25 ml of *M. charantia* F.E. was added to 100 ml of 1 mM $AgNO_3$ solution. After few minutes, brownish colour indicates formation of AgNPs. Solution mixture was left undisturbed in incubator for 24 h. UV-vis spectra confirmed the formation of AgNPs and then it was centrifuged (15,000 rpm, 25 min) for complete separation. Finally obtained precipitate was washed several times with DI water and double distilled ethanol, nanoparticle was carefully collected and dried to get final mass of AgNPs for further future experimentations and characterizations. This method was reported under optimised condition.

2.3. Characterization instruments

Green synthesized AgNPs were characterized via UV-Visible, Fourier transform infrared spectroscopy (FTIR), X-ray powder diffraction (XRD), Transmission electron microscopy (TEM), Scanning electron microscope (SEM) and Atomic-force microscopy (AFM). UV-vis spectra were recorded using Shimadzu UV 2450 to investigate optical properties based on unique surface Plasmon resonance at a wavelength of 300–800 nm. Crystalline nature and phase identification was done using X-ray diffractogram Shimadzu XRD 7000 with operating voltage 40KV, CuKα radiation (λ value 1.54060A°), current 30 mA and scan range 25–80°. Diffraction peaks of crystalline phases were compared with standard JCPDS data and average crystalline size was calculated using Debye-Scherrer's equation. FTIR were carried out by using Perkin Elmer Frontier, 91,579 in the range of 4000–400 cm^{-1} at a resolution of 4 cm^{-1} to identify possible functional biomolecules which acts as bio reducer, capping agent and stabilizer in the phyto fabrication of AgNPs. SEM was scanned by using JEOL JSM-7600F combined with EDX to study the size, shape and elemental composition of *M. charantia* capped AgNPs. For SEM, a drop of ultrasonicated colloidal AgNPs was dried over silicon wafer. Topographic information and SAED was obtained by Transmission electron microscopy PHILIPS TEM CM 200 at an accelerating voltage 200KV and resolution 0.24 nm. The sample was prepared by coating *M. charantia* colloidal AgNPs solution onto carbon coated copper grid using capillary tube. After two minutes, film was get deposited and extra solution was removed by using a blotting paper and TEM grid was dried completely before loading onto specimen holder. To reveal the actual surface topography and surface texture of biosynthesised AgNPs, AFM (atomic force microscopy) model name Bruker's Dimension Icon, USA was used in tapping mode with f (frequency) 50–90 kHz and K (cantilever's force constant) 0.4 N/m.

2.4. In vitro cytotoxicity assays

Sulforhodamine B (SRB) is a pink aminoxanthene dye used to assay rapid and sensitive measurement of drug-induced cytotoxicity. *In -vitro* cytotoxicity study was performed over A549 and HOP-62 cells using SRB assay [22]. Briefly A549 cells were grown in RPMI 1640 medium containing 10% fetal bovine serum and 2 ml L-glutamine. The cells were inoculated into 96 well microtiter plates in 100 μL medium. After cell inoculation, the micro plates were incubated at 37 °C in a 5% CO_2, 95% air and 100% relative humidity for 24 h. To evaluate anticancer efficiency of the *M. charantia* FE reduced AgNPs, the cultured cells were treated in

separate plates with different concentrations (10–80 μg/mL) of AgNPs and plates were incubated at standard conditions for 48 h and the assay was terminated by the addition of cold trichloroacetic acid (TCA). Further the cells were fixed in situ by the gentle addition of 50 μl of cold 30% (w/v) TCA (final concentration, 10% TCA) and incubated for 60 min at 4 °C. The supernatant was discarded, the plates were washed and dried until no standing moisture was visible. Sulforhodamine B (SRB) solution (50 μl) at 0.4% (w/v) in 1% CH_3COOH was added to each of the wells and then incubated for 20 min at room temperature.

After staining, unbound dye was recovered and the residual dye was removed by washing. Bound stain was eluted with 10 mM tris base, and the absorbance was read on a microplate reader (Tecan Infinite 200 PRO) at a wavelength of 540 nm (for maximum sensitivity) with 690 nm reference wavelength. The same procedure was repeated with HOP-62 cell line. Percentage growth inhibition was calculated using following formula -

$$\% \text{ cell inhibition} = 100 - \{(A_t - A_b)/(A_c - A_b)\} \times 100$$

where A_t is absorbance value of test compound, A_b is the absorbance value at blank and A_c is the absorbance value of control. Each treatment condition was replicated three times and morphology of the cells undergone cell death were recorded as images.

2.5. Statistical analysis

Data are reported as mean ± standard deviation of three replicates of each experiment. Results were analysed through one-way analysis of variance (ANOVA). Anova analysis of *M. charantia* supported AgNPs and *M. charantia* fruit extract is shown in Table 1. The results with $p < .05$ were considered to be statistically significant.

3. Results and discussions

3.1. Formation of M. Charantia mediated AgNPs and its optical properties

Transition of colour from light green to brown shows formation of silver nanoparticle. The surface plasmon resonance of AgNPs is completely shape and size dependent, which arises from the collective oscillation of the electrons in the conduction band from one surface of the particle to the other. The reduction of silver ion by *M. charantia* fruit extract and formation of AgNPs was monitored by UV-vis spectroscopy and represented in Fig. 1. Surface plasmon resonance absorption of AgNPs was obtained at 432 nm. Sathish Kumar and co-workers have demonstrated that maximum absorbance could be found at 435 nm due to presence of silver particle [23]. As per the statement of Mie's theory only single surface plasmon band arise due to spherical nanoparticle [24]. The number of peaks is inversely proportional to symmetry, and a single spherical morphology is expected according to UV-vis analysis.

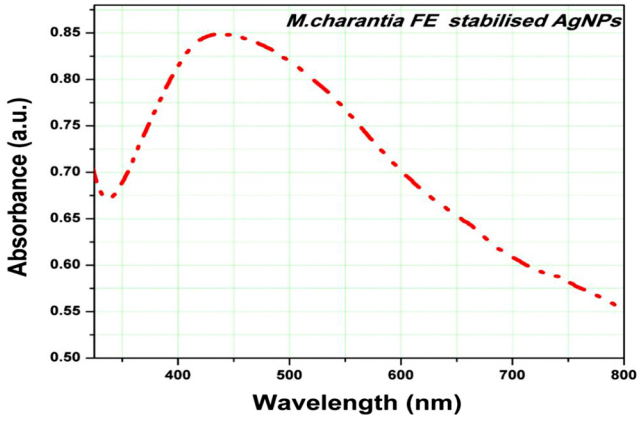

Fig. 1. UV-vis spectrum of *M. charantia* mediated AgNPs. The absorption spectra exhibited a strong broad peak at 432 nm.

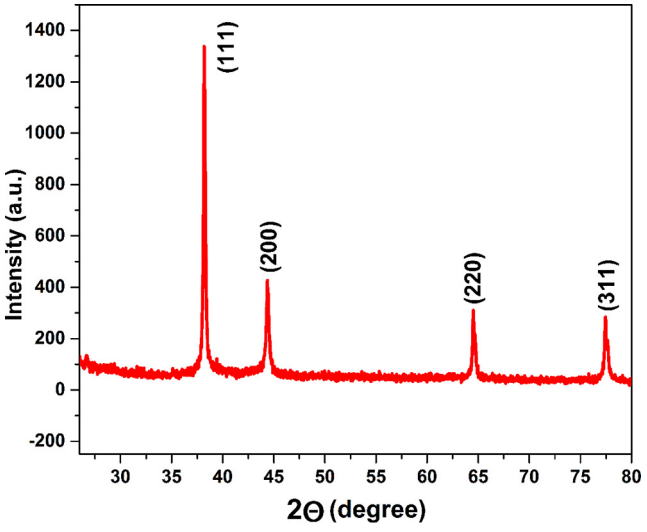

Fig. 2. X-ray diffractogram pattern of AgNPs corresponding to the diffraction from (1 1 1), (2 0 0), (2 2 0), (3 1 1) planes of fcc lattice, completely matched with JCPDS (04-0783) of silver nanoparticle with cubic symmetry.

3.2. Functional group identification

Involvement of surface functional relevant biomolecules of *M. charantia* FE, those interacted with metal surface and played an important role in reduction, capping and stabilisation, were recorded through FT-IR. Fig. 3 shows the FT-IR spectra acquired in the range of 4000–400 cm^{-1}. Fig. 3(a) represents FT-IR of *M. charantia* FE and *M. charantia* FE capped AgNPs is represented in Fig. 3 (b). The presence of intermolecular hydrogen bonding —OH was

Table 1
Comparison of biogenic AgNPs anticancer activity against A549 with previous reports.

Biogenic material for AgNPs synthesis	Size (nm)	Morphology	Anti-cancer (*in-viro* model) (μg/ml)	Dose (μg/ml)	IC_{50} (μg/ml)	Reference (et al.)
Cymodocea serrulate	5–25	Spherical	A549	10–100	100	Paaniappan [32]
Origanum vulgare	63–85	Spherical	A549	10–500	100	Sankar [33]
Rosa damascena	84 ± 10	Spherical	A549	20–120	80	Venkatasen [34]
Accorus calmus rhizome	31.83	Spherical	A549	25–175	53.2	Nakkala [35]
Helianthus Annus L	10–50	Spherical	A549	10–100	65	Thakore [36]
Syzygium samarangense	–	Spherical	A549	50–200	87.37	Thampi [37]
Enterococcus sp	10–80	Spherical	A549	1–100	100	Rajesh [38]
M. charantia FE	<13.85	Spherical	A549	10–80	**51.9**	This work

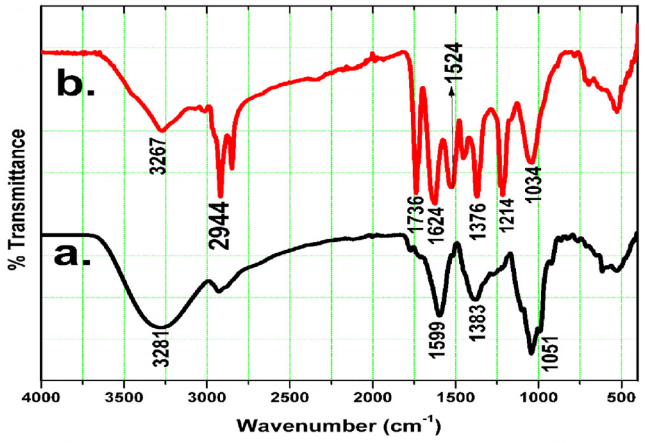

Fig. 3. (a). FTIR spectrum of (a) *M. charantia* fruit extract and (b) Bio synthesized *M. charantia* mediated AgNPs.

found at 3281 cm^{-1} in Fig. 3(a), which is shifted at 3267 cm^{-1} in AgNPs as observed in Fig. 3(b). Absorption peak from carbonyl group appears at 1599 cm^{-1}, whereas band at 1387 cm^{-1} observed due to primary amine groups and —C—O stretching mode [25]. Absorption band at 1051 cm^{-1} is due to C—N stretching vibration mode of amine [26]. In Fig. 3(b) of AgNPs FT-IR, band at 2944 cm^{-1} is due to presence of CH_2 asymmetric stretching, 1736 cm^{-1} is due to C=O stretching vibration, whereas the peak at 1624 cm^{-1} is due to N—H bending vibration of amine or amide I bonds of proteins. Band at 1524 cm^{-1} is attributed to C=C stretching. Some more shifting is observed at 1376 cm^{-1} which is attributed to C—N stretching of aromatic amine group [27–29], shifted from 1383 cm^{-1} of *M. charantia* fruit extract. Band at 1214 cm^{-1} indicating C—O—C stretching of ester and 1034 cm^{-1} represents C—N stretching vibration of primary amine. The huge shifting of absorption band from 3281 cm^{-1} of *M. charantia* FE to 3267 cm^{-1} in AgNPs occurs due to presence of —OH group, proves that polyphenol (flavonoid) plays important reducing agent in biosynthesis. Furthermore, shifting in aromatic amine group strongly indicates towards contribution of protein biomolecule. Presence of primary and secondary amine, which is building block of protein suggests that protein assist in stabilisation and acts as stabiliser and protector against agglomeration.

3.3. Formation and stabilisation mechanism of AgNPs

FTIR study reveals that polyphenols (flavonoids) are acting as strong reducing agent and contributing in reduction of Ag^+ to Ag^0 means flavonoids get oxidised during the reduction of Ag^+ to AgNPs. Since standard reduction potential of Ag^+/Ag^0 is 0.80 V, and standard reduction potential of quinone/phenol, aldehyde/alcohol and protein systems are less than 0.80 V ($E^0 < 0.80$ V), it implies that phenol and alcohol can act as strong reducing agent for the formation of *M. charantia* FE mediated AgNPs. The enol form of flavonoid gets converted into quinonoid form. This conversion involves removal of two hydrogen atoms from enol form and generation of quinonoid form with reduced two Ag^+ to Ag^0. Other phytocomponents of fruit extract such as protein, triterpene and secondary metabolites facilitates their formation, stabilisation and plays a critical role towards protection against agglomeration by fragmenting itself and consequently carboxylate group of proteins works as surfactant by developing a protein layer on nanoparticle and provides prolong stability (Fig. 5). It is evidenced from FT-IR which indicates involvement of —OH and —NH_2 groups and EDX studies that >C=O group of amino acid and peptide group

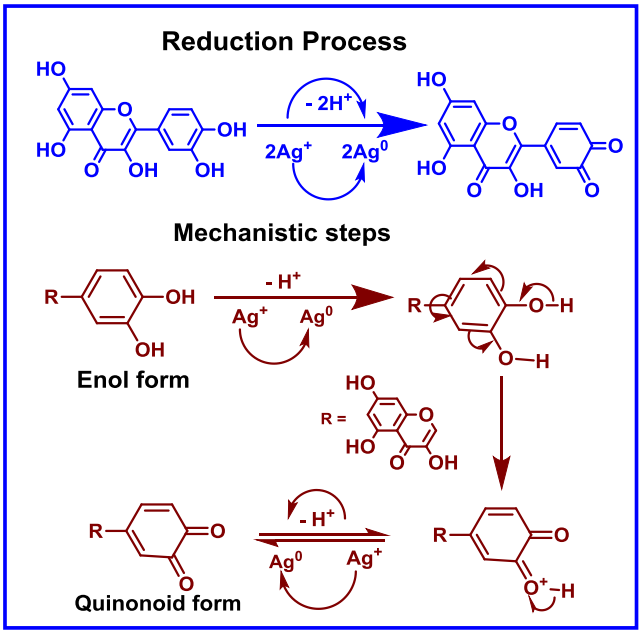

Fig. 4. Stepwise mechanistic details of the reduction process.

of proteins have strong chelating affinity to bind metal atom. They form a protecting cover and encapsulated around silver nanoparticles to inhibit the agglomeration and helps in stabilisation. Specifically, *M. charantia* fruit extract not only affects the size of AgNPs, it also works to protect and prevent AgNPs from being oxidised. The schematic plausible mechanistic chemistry of charge transfer induced molecular process in flavonoid during reduction of *M. charantia* mediated AgNPs is shown in Fig. 4.

3.4. Crystallographic analysis of M. Charantia FE mediated AgNPs

Nanocrystals of *M. charantia* FE mediated AGNPs formed was further evidenced by X-ray diffractogram analysis. Fig. 2 represents four characteristic bragg reflection peaks observed at 2θ values 38.2°, 44.2°, 64.7°, 77.4° corresponding lattice planes at (1 1 1), (2 0 0), (2 2 0), (3 1 1) with face centred cubic crystal (fcc) structure of metallic silver. The observed data were in tune with the standard diffraction data of silver with JCPDS 04-0783. The presence of bragg diffraction peaks signify high crystallinity and definite line broadening confirms particles are in nanoscale range. The (1 1 1) peak is most intense peak than others so it is a predominant orientation and average crystalline size was calculated by Debye Scherrer's equation [30] in which FWHM value was taken from highly intense (1 1 1) plane.

$$D = K\lambda/\beta\cos\theta, \text{ or } D = 0.94\lambda/\beta\cos\theta$$

where K is dimensionless space factor or Scherrer's constant (0.94), λ is the wavelength of Cu Kα radiation with value 0.1546 nm, β is full width at half maximum (FWHM) in radian and θ is Bragg angle. The calculated average crystalline size was found to be 12 nm having good consistency with the particle size observed in the TEM analysis.

3.5. Elemental composition analysis by EDS

To reveal elemental composition, green synthesized *M. charantia* FE stabilised AgNPs has been carried out using energy dispersive X-ray spectroscopy (EDX) mapping as shown in Fig. 7(d). Electromagnetic emission spectrum approximately at 3 KeV clearly confirms the strong characteristic presence of zero-valent silver

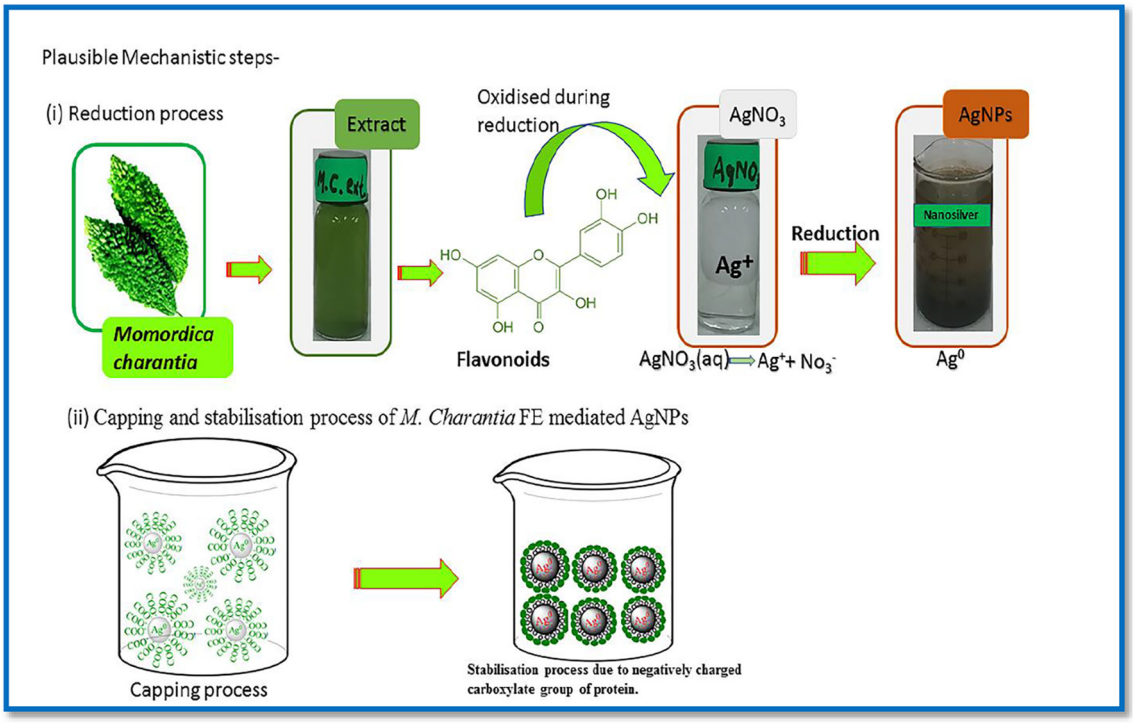

Fig. 5. The pictorial representation of the reduction, capping and stabilisation process of AgNPs using *M. charantia* fruit extract.

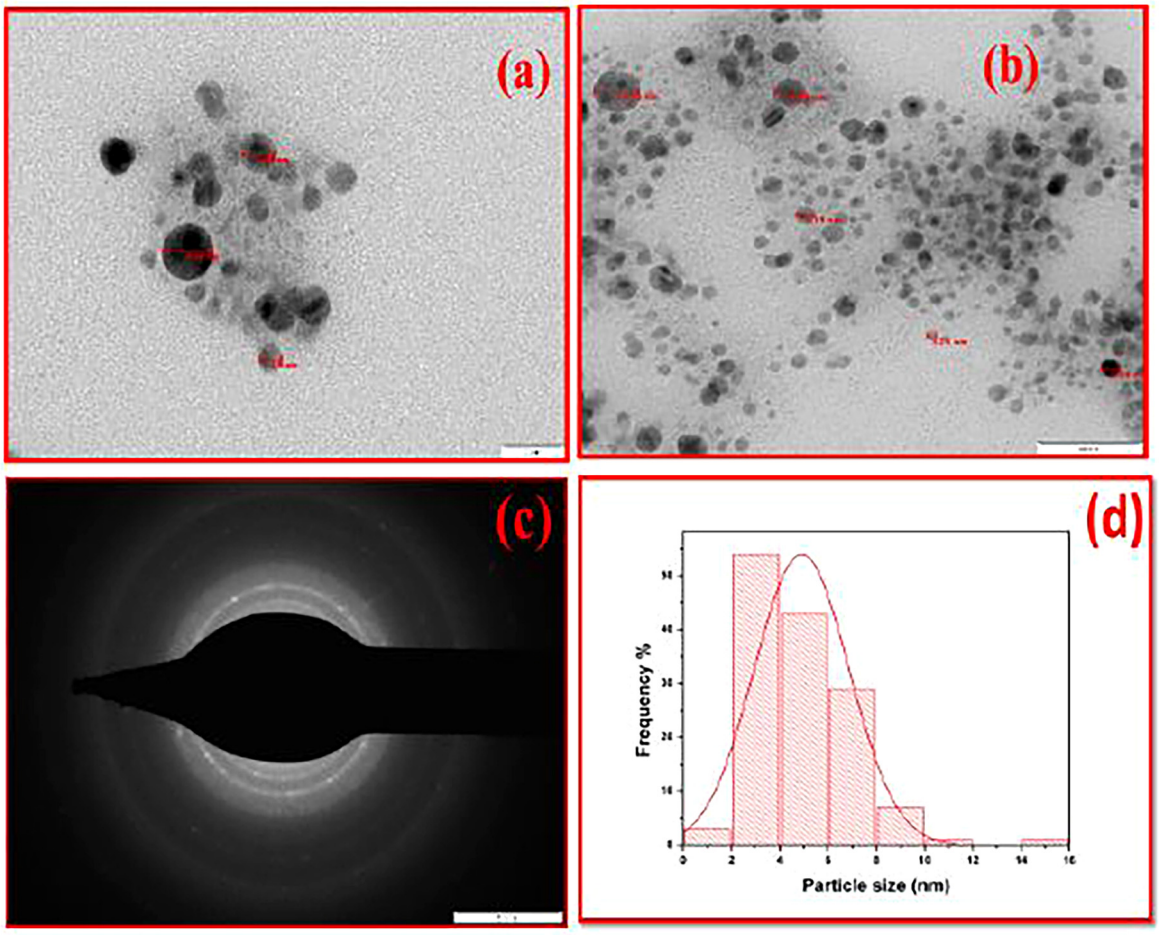

Fig. 6. Representative transmission electron microscopy (TEM) images of AgNPs (a and b) with spherical morphology under resolution of 20 nm and 50 nm scale (c) represents selected area electron diffraction pattern (d) represents frequency vs particle size distribution histogram of silver nanoparticles.

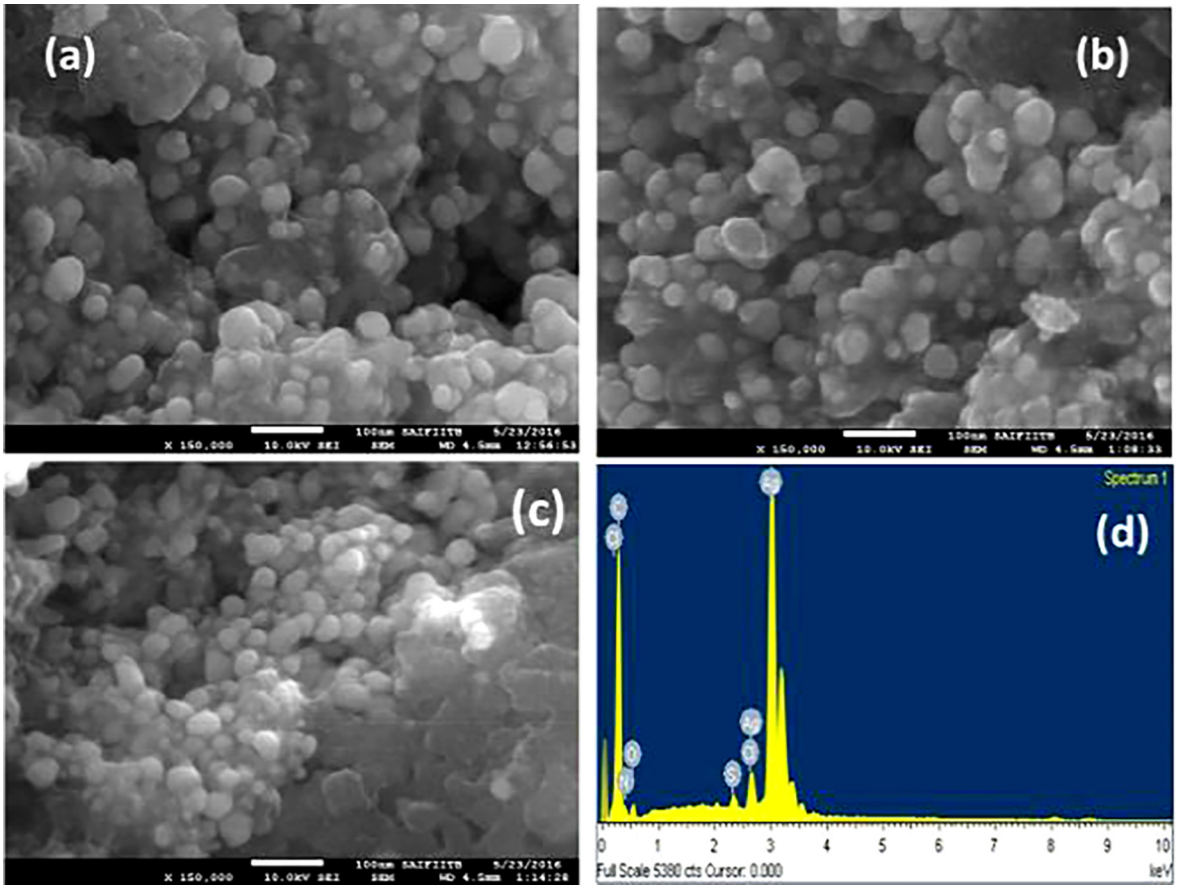

Fig. 7. (a–c) SEM micrograph showing morphology and Spherical shape of AgNPs synthesized using *M. charantia* fruit extract. (d) Represents EDX spectra confirming the presence of AgNPs at 3 Kev.

nanoparticle [31]. Presence of Cl (due to water) S, C, O and N may be due to protein biomolecule capping of *M. charantia* fruit extract that are bound to the surface of AgNPs.

3.6. Surface morphology of M. Charantia FE stabilised AgNPs

Surface morphology was investigated through SEM, TEM and AFM to understand the size, shape, distinct image of surface morphology and size distribution of *M. charantia* FE stabilised AgNPs. Fig. 7(a–c) shows SEM micrograph of *M. charantia* FE mediated AgNPs analysed in powder form. SEM analysis reveals the existence of highly scattered nanosphere, due to encapsulation of biomolecules some extent to variation in size is observed.

Spherical morphology of *M. charantia* FE stabilised AgNPs is also witnessed by AFM image shown in Fig. 8. To view the complete surface topography Fig. 8(a and b) represents whole and cropped projected (to view sidewise AgNPs distribution) 3D actual surface topography of uniformly distributed AgNPs on the glass substrate. Roughness, line profile, amplitude distribution function and bearing ratio curve are displayed in Fig. 8(c–f) respectively. In AFM, fine and dispersed spherical shaped silver nanoparticle ware observed with image average roughness 0.003 μm, maximum roughness peak height 0.026 μm, root-mean square roughness 0.004 μm, skewness −0.320 and profile length ratio was 1.004. A typical TEM micrograph is shown in Fig. 6(a and b) confirming spherical geometry, capped with active phytocomponents which prevented the nanoparticles from aggregation. Particles were well segregated, homogeneously distributed without any agglomeration shown under scale of 20 nm and 50 nm respectively. Fig. 6(d) represents frequency vs particle size distribution of Fig. 6(b). Intrinsic capping provides additional advantage in stabilization of silver nanoparticles. Fig. 6(c) represents selected area diffraction pattern recorded by aligning the electron beam perpendicular to the spherical facets of an individual nanosphere. The SAED pattern significantly confirms that AgNPs are polycrystalline in nature and diffraction rings are associated with the (1 1 1), (2 0 0), (2 2 0) and (3 1 1) crystal planes of pure face cantered cubic (fcc) structure of metallic silver nanoparticle which corroborate well with XRD diffractogram planes pattern. Morphological study indicates the formulation of spherical, homogeneously distributed, segregated, stable and polycrystalline silver nanoparticles from *M. charantia* fruit extract.

3.7. In-vitro testing for anticancer activity of AgNPs

The *in vitro* cytotoxic activity of *M. charantia* FE capped AgNPs were tested against human lung cancer cell lines by Sulforhodamine B (SRB) assay. This is the first report to evaluate *M. charantia* derived AgNPs cytotoxicity against lung cancer cell lines. Different concentrations of colloidal silver nanoparticles had been applied during treatment to check cell viability of A549 (Fig. 10) and HOP-62 (Fig. 11) human lung cancer cell lines. In the present study, IC_{50} (half maximum inhibitory concentration) of *M. charantia* FE against A549 holds at 102 μg/ml, while IC_{50} of AgNPs against A549 cells holds at 51.93 μg/ml. The IC_{50} value 51.93 μg/ml indicated greater biocompatibility as determined in previous reports against A549 cell line by earlier researchers [32–38] and presented in Table 1. In HOP-62 cell line, the observed IC_{50} value was 76.92 μg/ml, which indicates that as-synthesised AgNPs shows good

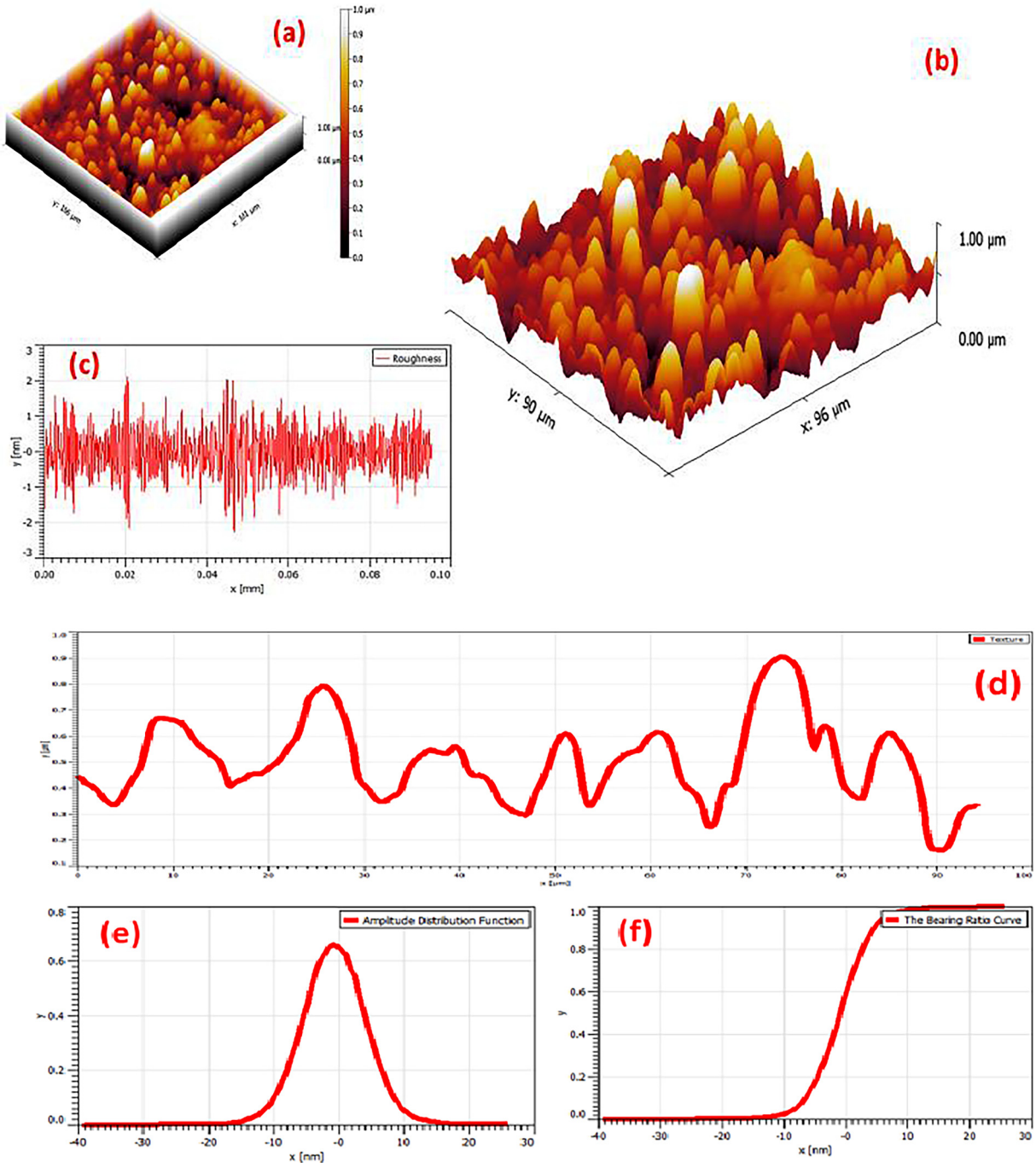

Fig. 8. Representative atomic force microscopy (AFM) images of *M. charantia* fruit extract stabilised AgNPs (a) and (b) represents overall and sidewise actual surface topography of uniformly distributed AgNPs on glass substrate (c) represents roughness profile (d) represents corresponding horizontal line profile (e) displays amplitude distribution function (f) represents bearing ratio curve.

anticancer activity against lung cancer cells. The anti-cancer efficacy of as synthesized AgNPs can be ordered as A549 > HOP-62 > *M. charantia* FE. A dose dependent decrease in the viability were observed on treatment with AgNPs confirms that AgNPs were successfully taken up by lung cancer cells. Fig. 9 displays the phase contrast microscopic images of control, positive control, *M. charantia* FE and AgNPs treated lung cancer cell line A549. Cytomorphological variations, which is a characteristic feature of cell death, such as cell burst, cell clumping, shrinkage and non-adherence to the surface, loss and disturbance in membrane stability were observed in A549 cells treated with 40 µg/ml FE and AgNPs. Statistical analysis of variance (ANOVA) are summarized in Table 2 and details of significant concentration was studied through Tukey test (see supplementary information).

A large number of *in vitro* studies provides evidence about biogenic AgNPs are highly cytotoxic for cancer cell in comparison to normal cell line. Recently, Du et al. observed cytotoxicity of plant mediated AgNPs on A549 cell (range 1–5 µg/ml) and found no cytotoxicity in normal Raw 264.7 (<2 µg/ml) [39]. Similarly, Singh et al. revealed that phyto-fabricated AgNPs showed toxicity against A549 and was non-toxic in Raw 264.7 [40]. Majeed et al. reported fungus-mediated AgNPs and investigated significant cytotoxic

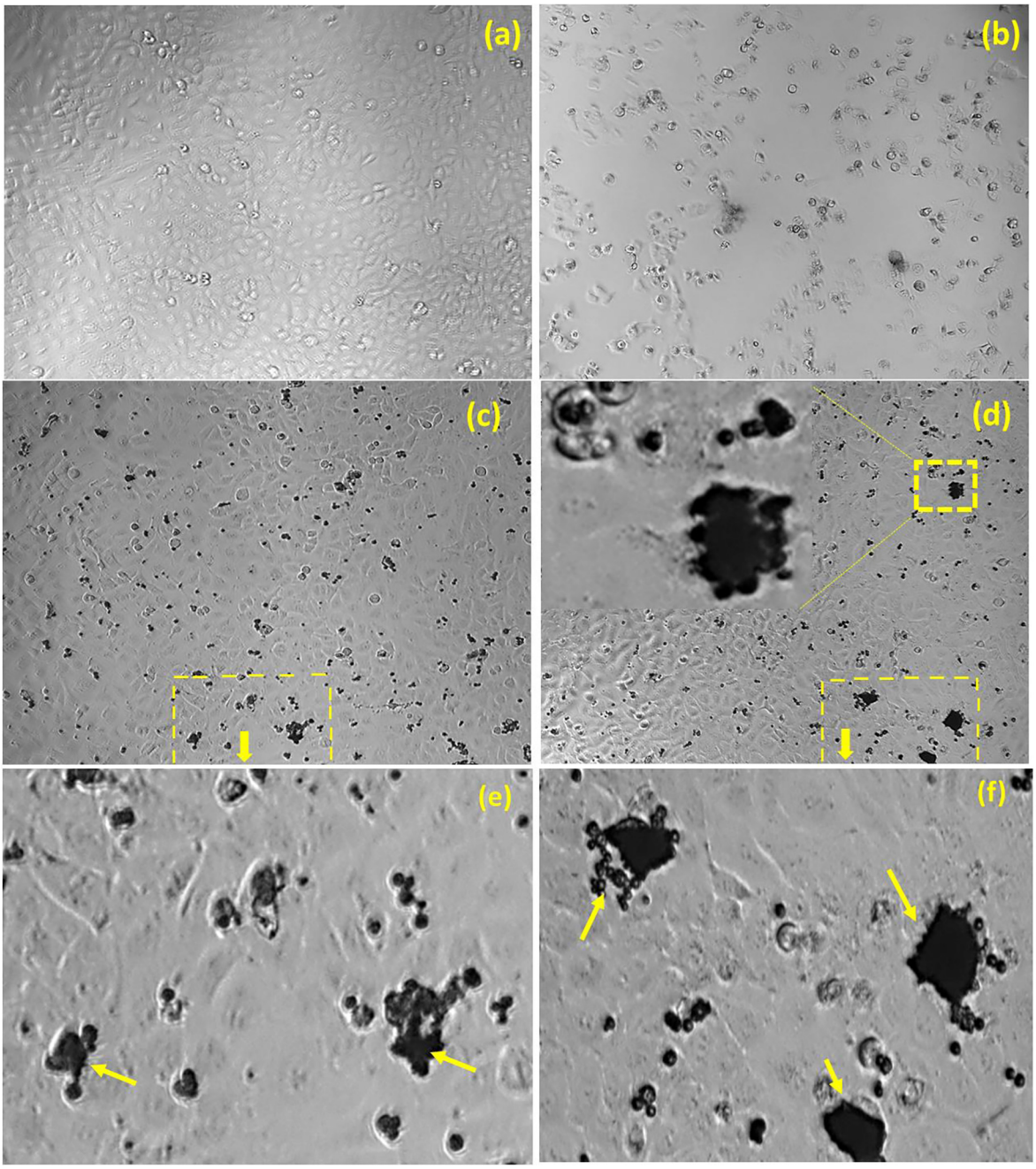

Fig. 9. *In-vitro* Cytomorphological features (phase contrast microscope images) of (a)-Control, (b)-Positive control (Adriamycin) (c) Cytomorphological modification observed during treatment of 80 μg/ml dose of M. charantia FE with A549 human lung cancer cells (d) Morphological changes associated with 80 μg/ml dose of synthesized silver nanodrug (marked portion of morphological variation of (c) and (d) is depicted in image (e) and (f) respectively).

potential in the range of 20–120 μg/ mL against A549, while 50% survival was demonstrated in the normal Vero cell line [41]. In addition, Kasithevar et al. reported biosynthesized AgNPs showed no cytotoxicity against vero cell lines even at high concentration of 200 μg/ml after 72 h of incubation [42]. These results provide conclusive evidence for cytotoxic effect of AgNPs on lung cancer cell rather than normal cell. Mechanistic path of AgNPs induced cytotoxicity is often mediated through generation of intracellular oxidative stress. Mitochondria release ROS, which leads to oxidative stress, these oxidative stress collapse antioxidant defence capacity and damage DNA which leads to apoptosis in cancer cell lines [43–46]. Several factors including size, morphology, surface charge, reactivity, reducing and capping agent are known to affect cytotoxic potential of AgNPs [47] and concentration of AgNPs plays major contribution in cytotoxicity. Present study suggests that *M. charantia* FE mediated AgNPs has tremendous potential to be used as a chemotherapeutic agent for lung cancer nanomedicine in near future.

4. Conclusion

In summary, we have designed a greener alternative for the synthesis of AgNPs in view of the environmental issues associated with conventional AgNPs preparation methods. In the present investigation, the synthetic protocol established was one-pot,

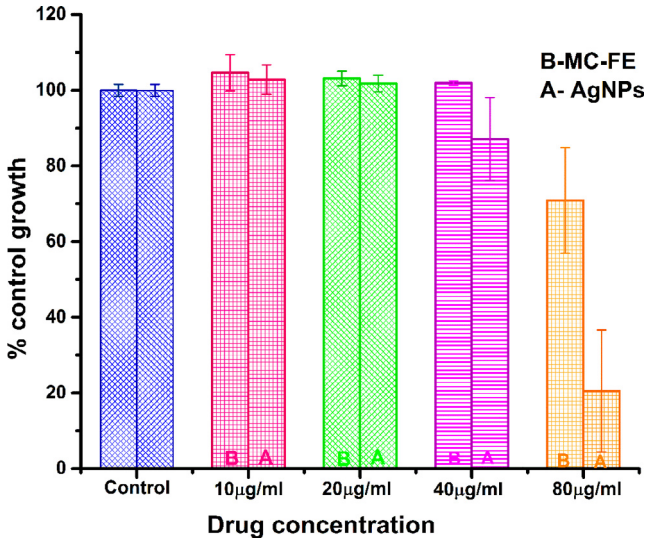

Fig. 10. *In-vitro* cytotoxicity studies for *M. charantia* fruit extract (MC-FE), which is represented by **B** and *M. charantia* stabilised silver nanoparticles (AgNPs), which is shown by **A**. In plot increasing concentration of AgNPs (10–80 μg/ml) (X-axis) inhibits the viability of cells (Y-axis). Statistical analysis was done by a one-way ANOVA, with Tukey's multiple comparisons post-test (available in supporting information). All the data were expressed in mean ± SD of three experiments and presented in Table 1.

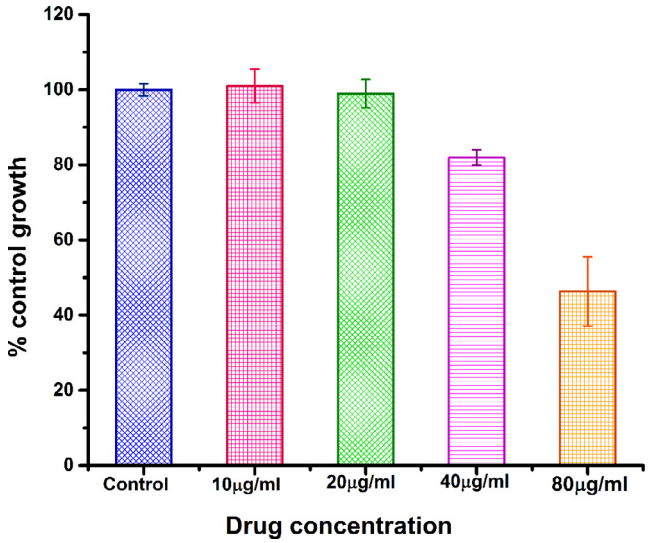

Fig. 11. *In-vitro* cytotoxicity study of *M. charantia* derived AgNPs against HOP-62 lung cancer cell line.

simple, clean, effective, eco-friendly, rapid, inexpensive and non-toxic. This synthetic approach ensures (1) environmentally benign procedure and (2) safe for clinical research. *M. charantia* fruit extract was successfully utilised as direct bioreductant, capping and stabilising agent for AgNPs fabrication as evidenced from FTIR. It may be inferred that phytocomponents present in *M. charantia* fruit extract specifically Flavonoid (polyphenol) played crucial role in reduction and organic protein layer worked as stabiliser. The mechanism of reduction process was also proposed. TEM observation confirmed the size of AgNPs < 13.85 nm. High consistency in spherical morphology was attested via TEM, FEG-SEM and AFM techniques. Cytotoxic results show *M. charantia* FE mediated AgNPs (IC_{50} = 51.93 μg/ml) are more biocompatible in comparison to *M. charantia* FE (IC_{50} = 102 μg/ml). In addition, synthesized AgNPs have shown better anticancer property while treated with A549 ((IC_{50} = 51.93 μg/ml) in comparison to HOP-62 ((IC_{50} = 76.92 μg/ml). The present investigation showed synthesized silver nanoparticles induce a dose dependent inhibition activity against A549 and HOP-62 human lung carcinoma. Inexpensive and room temperature synthesis of AgNPs from *M. charantia* FE and their fitness for exploitation in bio-responsive theranostics material against lung cell have been demonstrated successfully for the first time. The results provide critical evidence of *M. charantia* fruit extract derived AgNPs to achieve designated goal in cytotoxic applications against lung cancer cells. We believe that our finding extends the application of AgNPs in nanomedicine research to design efficient nanocarrier for targeted drug delivery and treatment.

Disclosure

The authors report no conflict of interest in this work.

Table 2
Anova analysis of (2a). AgNPs against A549 (2b). *M. charantia* FE against A549 and (2c). AgNPs against HOP-62 human lung cancer cell lines.

2a. Dose dependent effect of *M. charantia* fruit extract stabilised AgNPs on A549 human lung cancer cell line. Statistical analysis is based on One-way ANOVA at 5% level of significance					
ANOVA analysis of M. charantia stabilized AgNPs against A549					
AgNps Concentrations	10	20	40	80	Pooled std. deviation
Mean	102.8	101.76	87.03	20.46	17.30
SD	6.76	3.81	18.45	27.87	
95%CI	102.8 ± 16.79	101.76 ± 9.46	87.03 ± 45.83	20.46 ± 56.81	
2b. ANOVA analysis of M. Charantia fruit extract against A549					
M. charantia FE conc.	10	20	40	80	Pooled std. deviation
Mean	104.56	103.06	101.83	70.93	12.84
SD	8.3	3.239	1.001	24.105	
95% CI	104.56 ± 20.62	103.06 ± 8.04	101.83 ± 2.48	70.93 ± 59.88	
2c. ANOVA analysis of M. charantia stabilized AgNPs against HOP-62					
AgNps Concentrations	10	20	40	80	Pooled std. deviation
Mean	101.03	98.93	82.03	46.33	9.60
SD	7.74	6.58	3.50	15.91	
95% CI	101.03 ± 19.22	98.93 ± 16.34	82.03 ± 8.69	46.33 ± 39.52	

*Coeff Var = 0.2217, Root MSE = 17.29603, Data mean = 78.01.
*Coeff Var = 0.13522, Root MSE = 12.89566, Data mean = 95.1.
*Coeff Var = 0.32546, Root MSE = 26.70, Data mean = 82.05.

Acknowledgements

Minakshi Jha acknowledges university grants commission (UGC), New Delhi, India, for financial support. I would like to gratefully acknowledge SAIF, IIT Mumbai for FEG-SEM, TEM and ACDSF, ACTREC for anticancer studies.

Appendix A. Supplementary material

Supplementary data associated with this article can be found, in the online version, at https://doi.org/10.1016/j.jgeb.2017.12.001.

References

[1] Rao CNR, Müller A, Cheetham AK, editors. The chemistry of nanomaterials. Synthesis, properties and applications, vols. 1 and 2. Weinheim: Wiley-VCH Verlag; 2004.
[2] Li H, Xu D. Silver nanoparticles as labels for applications in bioassays. Trends Anal Chem 2014;61:67–73.
[3] Ridge CA, Mcerlan AM, Ginsberg MS. Epidemiol. Lung Cancer 2013;30(2):93–8.
[4] American Cancer Society. Cancer facts & figures, Atlanta; 2014.
[5] Hannun YA. Apoptosis and the dilemma of cancer chemotherapy. Blood 1997;89:1845–53.
[6] Lukyanov AN, Torchilin VP. Micelles from lipid derivatives of water-soluble polymers as delivery systems for poorly soluble drugs. Adv Drug Deliv Rev 2004;56(9):1273–89.
[7] Kipp JE. The role of solid nanoparticle technology in the parenteral delivery of poorly water-soluble drugs. Int J Pharm 2004;284:109–22.
[8] Gao S, Zhang Z, Liu K, Dong B. Direct evidence of plasmonic enhancement on catalytic reduction of 4-nitrophenol over silver nanoparticles supported on networks. Appl Catal B 2016;188:245–52.
[9] Taglietti A, Fernandez D, et al. Antibacterial activity of glutathione-coated silver nanoparticles against gram positive and gram-negative bacteria. Langmuir 2012;28:8140–8.
[10] Rai M, Yadav A, Gade A. Silver nanoparticles as a new generation of antimicrobials. Biotechnol Adv 2009;27:76–83.
[11] Choi H, Ko S, et al. Versatile surface plasmon resonance of carbon-dot-supported silver nanoparticles in polymer optoelectronic devices. Nat Photonics 2013;7:732–8.
[12] Gutierrez FM, Olive PL, Banuelos A, Orrantia E, et al. Synthesis, characterization and evaluation of antimicrobial and cytotoxic effect of silver and titanium nanoparticles. Nanomedicine 2010;6:681–8.
[13] Patra S, Mukharjee S, et al. Green synthesis, characterization of gold and silver nanoparticles and their potential application for cancer therapeutics. Mater Sci Eng, C 2015;53:298–309.
[14] Xia QH, Ma YJ, Wang JW. Biosynthesis of silver nanoparticles using *Taxus Yunnanensis Callus* and their antibacterial activity and cytotoxicity in human cancer cells. Nanomaterials 2016;6(9):160.
[15] Jang SJ, Yang IJ, et al. In-vitro anticancer activity of green synthesized silver nanoparticles on MCF-7 human breast cancer cells. Mater Sci Eng, C 2016;68:430–5.
[16] Gade A, Gaikwad S, Duran N, Rai M. Green synthesis of silver nanoparticles by *Phoma glomerata*. Micron 2014;59:52–9.
[17] Nayak D, Ashe S, et al. Bark extract mediated green synthesis of silver nanoparticles: evaluation of antimicrobial activity and antiproliferative response against osteosarcoma. Mater Sci Eng, C 2016;58:44–52.
[18] Mittal AK, Bhaumik J, et al. Biosynthesis of silver nanoparticles: elucidation of prospective mechanism and therapeutic potential. J. Colloid Interface Sci. 2014;415:39–47.
[19] Kubola J, Siriamornpun S. Phenolic contents and antioxidant activities of bitter gourd *(Momordica charantia* L) leaf, stem and fruit fraction extracts in vitro. Food Chem 2008;110(4):881–90.
[20] Gandhiraj V, Sathish Kumar K, Madhu sudhanan J, et al. Antitumor activity of biosynthesized silver nano particles from leaves of *Momordica charantia* against MCF-7 cellline. Int J Chem Tech Res 2015;8(7):351–62.
[21] Ajita B, Reddy YAK, et al. Biosynthesis of silver nanoparticles using *Momordica charantia* leaf broth: Evaluation of their innate antimicrobial and catalytic activities. J Photochem Photobiol, B 2015;146:1–9.
[22] Vichai V, Kirtikara K. Sulforhodamine B colorimetric assay for cytotoxicity screening. Nat Protoc 2006;1(3):1112–6.
[23] Sathish kumar M, Sneha K, et al. Cinnamon zylanicum bark extract and powder mediated green synthesis of nano-crystalline silver particles and its bactericidal activity. Colloids Surf B Biointerfaces 2009;73(2):332–8.
[24] Ghaforyan H, Ebrahimzadeh M, et al. Study of the Optical Properties of Nanoparticles using Mie Theory world appl. Programming 2015;5(4):79–82.
[25] Zhang G, Du M, Li Q, et al. Green synthesis of Au–Ag alloy nanoparticles using *Cacumen platycladi* extract. RSC Adv 2013;3:1878–84.
[26] Shihab RN, Al-Kalifaw EJ. Environmental friendly synthesis of silver nanoparticles using leaf extract of Mureira Tree (*Azadirachta indica*) cultivated in Iraq and efficacy the antimicrobial activity. J Nat Sci Res 2016;6 (4):2224–3186.
[27] Thanaa I, Ola A, Gihan A, et al. Green synthesis of silver nanoparticle: synthesis, characterization and antibacterial activity. Nanosci Nanotechnol 2015;5(2):23–9.
[28] Reena singh et al. Biosynthesis of silver nanoparticles by marine invertebrate (polychaete) and assessment of its efficacy against human pathogen. J Nanoparticles 2014; 718240.
[29] Sudipnath et al. Silver organosol: synthesis, characterization and localized surface plasmon resonance study. New J Chem 2005;29:1527–34.
[30] Loo YY, Chieng BW, et al. Synthesis of silver nanoparticles by using tea leaf extract from *camellia Sinensis*. Int J Nanomed 2012;7:4263–7.
[31] Agnihotri S, Mukharji S, et al. Size- controlled silver nanoparticles synthesized over the range 5–100 nm using the same protocol and their antibacterial efficacy. RSC Adv 2014;4:3974–83.
[32] Paaniappan P, Satishkumar G, Sankar R. Fabrication of nano-silver particles using *Cymodocea serrulata* and its cytotoxicity effect against human lung cancer A549 cells line. Spectrochim Acta Part A Mol Biomol Spectrosc 2015;138:885–90.
[33] Sankar Renu et al. *Origanum Vulgare* mediated biosynthesis of silver nanoparticles for its antibacterial and anticancer activity. Colloids Surface B: Biointerfaces 2013;108:80–4.
[34] Venkatesan B, et al. Rapid synthesis of biocompatible silver nanoparticles using aqueous extract of Rosa damascena petals and evaluation of their anticancer activity. Asian Pac J Trop Med 2014; 7S1: p. S294–300.
[35] Nakkala JR et al. Biological activities of green silver nanoparticles synthesized with *Acorous calmus* rhizome extract. Eur J Med Chem 2014;85:784–94.
[36] Thakore S, Rathore PS, Jadeja RN, Thounaojam M, Devkar RV. Sunflower oil mediated biomimetic synthesis and cytotoxicity of monodisperse hexagonal silver nanoparticles. Mater Sci Eng, C 2014;44(5):209–15.
[37] Thampi N, Shalini JV. Bio-Prospecting the in-Vitro antioxidant and anti-Cancer activities of Silver Nanoparticles synthesized from the leaves of syzygium samarangense. Int J Pharmacy Pharm Sci 2015;7(7):269–74.
[38] Rajeshkumar S, Malarkodi C, Vanaja M, Annadurai G. Anticancer and enhanced antimicrobial activity of biosynthesizd silver nanoparticles against clinical pathogens. J Mol Struct 2016;1116(55):165–73.
[39] Du J, Singh H, Yi TH. Antibacterial, Anti-Biofilm and Anticancer potentials of green synthesized silver nanoparticles using *Benzoin gum* (Styrax Benzoin) extract. Bioprocess Biosyst Eng 2016;39(12):1923–31.
[40] Singh H, Du J, Yi TH. Green and rapid synthesis of silver nanoparticles using *Borago Officinalis* leaf extract: Anticancer and Antibacterial activities. Artif Cells Nanomed Biotechnol 2016;45(7):1310–6.
[41] Majeed S, bin Abdullah MS, Dash GK, Ansari MT, Nanda A. Biochemical synthesis of silver nanoparticles using Filamentous Fungi *Penicillium Decumbens* (MTCC-2494) and its efficacy against A-549 lung cancer cell line. Chin J Nat Med 2016;14(8):615–20.
[42] Kasithevar M, Saravanan M, Prakash P, Kumar H, Ovais M, Barabadi H, et al. Green synthesis of Silver nanoparticles using Alysicarpus Monilifer leaf Extract and its Antibacterial Activity Against MRSA and CoNS Isolates in HIV Patients. J Interdiscip Nanomed 2017; 2, 2 (2017): p. 131–41.
[43] Han JW, Gurunathan S, Jeong JK, Choi YJ, et al. Oxidative stress mediated cytotoxicity of biologically synthesized silver nanoparticles in human lung epithelial adenocarcinoma cell line. Nanoscale Res Lett 2014;9:459.
[44] Awasthi KK, Awasthi A, Kumar N, Awasthi K, et al. Silver nanoparticle induced cytotoxicity, oxidative stress and DNA damage in CHO cells. J Nanopart Res 2013;15:1898.
[45] Yang W, Shen C, et al. Food storage material silver nanoparticles interfere with DNA replication fidelity and bind with DNA. Nanotechnology 20(8), 085102.
[46] Xi F, Zhang W, Shen S. Gurunathan, Silver nanoparticle-mediated cellular responses in various cell lines: an in vitro model. Int J Mol Sci 2016;17 (10):1603.
[47] Gurunathan S, Jeong JK, Han JW, Zhang XF, Park JH, Kim JH. Multidimensional effects of biologically synthesized silver nanoparticles in *Helicobacter pylori*, *Helicobacter felis*, and human lung (L132) and lung carcinoma A549 cells. Nanoscale Res Lett 2015;10:1–17.